Journal of Neural Engineering

PAPER

A murine model of a novel surgical architecture for proprioceptive muscle feedback and its potential application to control of advanced limb prostheses

To cite this article: Tyler R Clites *et al* 2017 *J. Neural Eng.* **14** 036002

View the article online for updates and enhancements.

Related content

- In vivo characterization of regenerative peripheral nerve interface function
Daniel C Ursu, Melanie G Urbanchek, Andrej Nedic et al.
- Influence of nerve cuff channel count and implantation site on the separability of afferent ENG
Carolina Silveira, Emma Brunton, Sally Spendiff et al.
- Chronic recording of hand prosthesis control signals via a regenerative peripheral nerve interface in a rhesus macaque
Z T Irwin, K E Schroeder, P P Vu et al.

Recent citations

- Proprioception from a neurally controlled lower-extremity prosthesis
Tyler R. Clites *et al*
- On prosthetic control: A regenerative agonist-antagonist myoneural interface
S. S. Srinivasan *et al*

This content was downloaded from IP address 129.100.58.76 on 14/06/2018 at 13:33

IOP Publishing Journal of Neural Engineering
J. Neural Eng. **14** (2017) 036002 (12pp) https://doi.org/10.1088/1741-2552/aa614b

A murine model of a novel surgical architecture for proprioceptive muscle feedback and its potential application to control of advanced limb prostheses

Tyler R Clites[1], Matthew J Carty[1,2], Shriya Srinivasan[1], Anthony N Zorzos[1] and Hugh M Herr[1,3]

[1] Center for Extreme Bionics, Massachusetts Institute of Technology, Cambridge, MA, United States of America
[2] Department of Plastic and Reconstructive Surgery, Brigham and Women's Hospital, Boston, MA, United States of America

E-mail: hherr@media.mit.edu

Received 18 November 2016, revised 15 February 2017
Accepted for publication 17 February 2017
Published 14 March 2017

Abstract

Objective. Proprioceptive mechanisms play a critical role in both reflexive and volitional lower extremity control. Significant strides have been made in the development of bionic limbs that are capable of bi-directional communication with the peripheral nervous system, but none of these systems have been capable of providing physiologically-relevant muscle-based proprioceptive feedback through natural neural pathways. In this study, we present the agonist–antagonist myoneural interface (AMI), a surgical approach with the capacity to provide graded kinesthetic feedback from a prosthesis through mechanical activation of native mechanoreceptors within residual agonist–antagonist muscle pairs. *Approach.* (1) Sonomicrometery and electroneurography measurement systems were validated using a servo-based muscle tensioning system. (2) A heuristic controller was implemented to modulate functional electrical stimulation of an agonist muscle, using sonomicrometric measurements of stretch from a mechanically-coupled antagonist muscle as feedback. (3) One AMI was surgically constructed in the hindlimb of each rat. (4) The gastrocnemius-soleus complex of the rat was cycled through a series of ramp-and-hold stretches in two different muscle architectures: native (physiologically-intact) and AMI (modified). Integrated electroneurography from the tibial nerve was compared across the two architectures. *Main results.* Correlation between stretch and afferent signal demonstrated that the AMI is capable of provoking graded afferent signals in response to ramp-and-hold stretches, in a manner similar to the native muscle architecture. The response magnitude in the AMI was reduced when compared to the native architecture, likely due to lower stretch amplitudes. The closed-loop control system showed robustness at high stretch magnitudes, with some oscillation at low stretch magnitudes. *Significance.* These results indicate that the AMI has the potential to communicate meaningful kinesthetic feedback from a prosthetic limb by replicating the agonist–antagonist relationships that are fundamental to physiological proprioception.

Keywords: proprioception, afferent feedback, prosthetic control, amputation, peripheral nerve interface, bionics, surgery

(Some figures may appear in colour only in the online journal)

[3] Author to whom any correspondence should be addressed.

 © 2017 IOP Publishing Ltd Printed in the UK

1. Introduction

In the United States, over 500 000 people live with lower extremity loss [1] and 130 000 lower extremity amputations are carried out annually [2]. In order to restore stable and independent ambulation, and improve the quality of life for persons with lower extremity amputation, advanced prosthetic joint devices have been developed (e.g. [3–9]). Normalization of function for individuals with lower extremity amputation is within reach, and direct communication between neural implants and biomimetic, external prosthetic devices represents a crucial step forward.

Current clinical amputation procedures date back to the Civil War era, and are designed to prepare the residuum for fitting of a prosthetic socket [10]. In the current surgical paradigm, distal residual muscle tissues are fixed isometrically as to create padding for the distal end of the residuum. End organs and other tissues distal to the amputation site are discarded. The distal ends of amputated nerves are usually buried into fat tissue or deep into the residual limb to protect them from mechanical stimulation, which might otherwise cause painful sensations [11]. State- of-the-art approaches to peripheral nerve interfacing have been developed within the bounds of this dated amputation paradigm, working to extract efferent signals from and reproduce afferent signals in transected peripheral nerves that are buried deep within the residual tissues [12, 13]. The subset of afferent signals responsible for proprioceptive sensation has remained particularly elusive in these interfacing modalities.

Proprioception is essential to motor control, functional joint stability, and gait adaptation [14, 15]. Although neuroscience research has documented the contributions of various biological mechanoreceptors to proprioceptive sensation, including joint receptors (e.g. [16–18]) and cutaneous sensory receptors (e.g. [19–22]), evidence points to muscle spindle afferents as predominant mediators of joint kinesthesia [23–25]. It is well understood that muscle spindle afferents discharge proportionally to changes in muscle length and velocity (e.g. [26–29]). Primary spindle afferent response is best characterized by ramp-and-hold stretches, with discharge rates proportional to stretch velocity and magnitude. Secondary spindle afferent response is largely proportional to stretch magnitude, with a lower dynamic sensitivity (e.g. [30–33]). Although muscle afferents represent only a portion of the larger proprioceptive system, studies in vibratory-induced illusory kinesthesia have indicated that preservation of functional muscle stretch relationships is sufficient to promote sensations of joint kinesthesia (e.g. [34–36]). This assertion is further bolstered by the preservation of kinesthesia in patients having orthopedic joint replacement surgery [37], during which the physiological joint capsule in its entirety was removed. The same phenomenon has been observed in patients having lost neural connectivity to cutaneous and joint capsule receptors secondary to severe dorsal column injury, who report intact position and movement sensibility [38, 39]. For a complete discussion of the roles of the various afferent receptors in proprioception, we refer the reader to [23].

The architecture explored in this study is designed to preserve the complex patterns of muscle receptor discharge responsible for kinesthetic sensation, by replicating basic muscle relationships. The fundamental motor unit to control a biological joint is an agonist–antagonist muscle-tendon pair. Such a muscle-tendon relationship allows for simultaneous control of joint state (position and speed) and impedance (stiffness and damping) for upper and lower extremity motor tasks. At least one pair of antagonistic muscles is needed for each degree of freedom of a limb in order to control joint state, torque, and impedance [40]. Evidence suggests that proprioceptive feedback of joint positioning is largely dependent on the dynamic relationship between muscle spindle afferents in agonist and antagonist muscle groups acting simultaneously on the same degree of freedom [36, 41]. When a muscle on one side of a biological joint contracts (e.g. the 'agonist') and moves the joint, this motion elongates the muscle ('antagonist') that is attached to the opposite side of the joint and causes the antagonist spindle afferent receptors to discharge. Similarly, if contraction of the antagonist causes the joint to rotate in the opposite direction, then the agonist will be elongated, causing the agonist spindle receptors to discharge [36].

Unfortunately, translation of externally-produced sensory data from prostheses into biologically compatible feedback that is perceived by the amputee as normal proprioception has, to date, been unsuccessful. Vibration-induced illusory kinesthesia [35, 42] has been explored as a means of providing joint state information through activation of cutaneous stretch receptors, but translation of this approach has been a major hurdle, due in part to its reliance on mechatronic hardware mounted to the surface of the skin. Direct peripheral nerve stimulation through implantable cuff electrodes has recently been shown effective in providing cutaneous touch perception, but proprioceptive sensation has remained an area of difficulty [43]. It is our belief that prior efforts to recapitulate proprioceptive sensory feedback have proven difficult due primarily to their uniform neglect to incorporate the end terminal biological mediators innate to the biological human limb.

As an alternative to these prior approaches, we herein demonstrate the agonist–antagonist myoneural interface (AMI), a novel amputation paradigm and implant architecture that leverages existing end organs and their natural neural pathways for provision of robust, physiologically-relevant proprioceptive feedback. The amputation model described is unique in its capacity to utilize native tissue mechanoreceptors to translate prosthetic sensory information related to muscle stretch and tension into neural signals similar to those experienced in the normal biological milieu. This work represents a first step toward validation of the AMI concept; the fundamental advancement presented herein is a murine model of the series coaptation of natively-innervated agonist–antagonist muscle pairs. In this animal model, we demonstrate the utility of sonomicrometery in enabling closed-loop control of muscle stretch in both the native and AMI architectures, and present neural signals indicating the potential of the AMI to provide graded muscle state feedback.

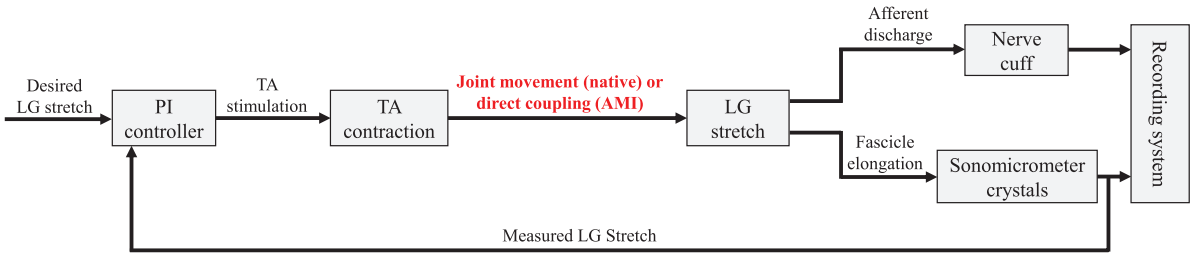

Figure 1. Experimental system overview. Stimulation of the TA was modulated by a proportional-integrative controller, with difference between desired LG stretch and sonomicrometric measurement of actual LG stretch serving as the error signal. Motion from the TA was transduced to LG stretch, and measurements of LG afferent activity and fascicle elongation were recorded.

2. Materials and methods

2.1. Rationale

Standard amputation paradigms do not allow for physiologically-relevant proprioceptive feedback because the innervated residual muscles are held isometric, and force on any given residual muscle is not modulated by an antagonist muscle. The AMI approximates physiological proprioceptive mechanisms by incorporating residual muscles from discrete agonist–antagonist muscle pairs (e.g. gastrocnemius and tibialis anterior) in series. Contraction of the agonist muscle via the standard motor efferent nerve activates the native contractile mechanoreceptors in the agonist muscle, as well as the native intrafusal muscle spindle stretch fibers of the mechanically-coupled antagonist muscle, both of which provide afferent proprioceptive signaling through the sensory components of their respective innervation nerves. Subsequent activation of the antagonist stimulates a complimentary stretch on the agonist; as such, the AMI has the capacity to reproduce a physiologically relevant agonist–antagonist mechanical coupling, providing non-isometric fascicle strains and agonist-antagonist fascicle state spindle feedbacks.

Effective implementation of the AMI as a means of communicating proprioceptive information from an external limb prosthesis to the nervous system depends primarily on two essential, non-obvious advancements. We present developments in each of these areas, which include:

1. closed-loop stimulation control with reliable, real time muscle-state feedback, and
2. a surgical geometry that provides sufficient agonist-antagonist coupling to evoke a graded spindle response.

The study here presented was designed to validate these components, and to demonstrate efficacy of the systems-level integration thereof in a murine model. The full experimental system from this study is shown in figure 1. A proportional-integrative controller was used to modulate stimulation of the tibialis anterior (TA) to enforce a desired lateral gastrocnemius (LG) stretch. Electroneurography (ENG) from LG motor afferents was recorded via a nerve cuff placed on the tibial nerve. LG muscle stretch was recorded via sonomicrometery crystals, and used to inform the stimulation controller. In this paper we first describe a measurement validation procedure, which was carried out to ensure robustness in the ENG and sonomicrometery recording systems, as well as to establish a baseline for graded motor afferent response to LG muscle stretch. We then present results from two experimental paradigms. The first, which serves as a positive control, evaluated the afferent response of the LG to stretch induced by functional electrical stimulation (FES) of the antagonist TA, with both muscles in their native orientations. The second experiment was a reproduction of the first, with a surgical modification to the muscle geometry wherein an AMI was constructed and movement was transduced through direct mechanical coupling of the muscles.

2.2. Animals and measurement system preparation

All animal care and procedures were conducted in accordance with the *Guide for the Care and Use of Laboratory Animals*. In these acute experiments, each of 10 male 4.5 months old Lewis rats (381 $\pm$ 9 g), was anesthetized under an isoflurane/oxygen gas mixture at 1–2% isoflurane. A 5 cm incision was made on the lateral aspect of the left distal hindlimb. The biceps femoris was disinserted at the knee, and retracted to reveal the common peroneal and tibial branches of the sciatic nerve. A custom tri-polar nerve cuff was sutured in place on the tibial branch.

Sonomicrometery has long been used in the field of biomechanics to measure muscle elongation. This technology utilizes ultrasound time-of-flight from a pair of implanted piezoelectric crystals to provide a direct measurement of muscle fascicle length [44–46]. A pair of 1 mm sonomicrometery crystals (Sonometrics) was inserted into the LG. The procedure for this is as follows: first, a pocket was created for each crystal by piercing the epimysial fascia of the muscle with small pointed scissors. The proximal crystal was then positioned at the proximal musculotendous junction of the corresponding muscle; the distal crystal was placed approximately 1 cm distal to the proximal crystal, along the muscle line of action. Crystal alignment was manipulated to maximize signal-to-noise ratio, while monitoring crystal output via the sonomicrometry amplifier (UDG, Sonometrics) and oscilloscope (TDS 2002, Tektronix) during implantation. The crystals were secured in place by closing the pockets and suturing the lead wires to the muscle surface with 5-0 nylon suture. The ankle joint was then suspended from above, via 5-0 nylon suture attached to a base-mounted spring clamp, and the foot was manually cycled through its full range of motion while sonomicrometery data were recorded. Rest position was defined as the equilibrium ankle joint position in the absence

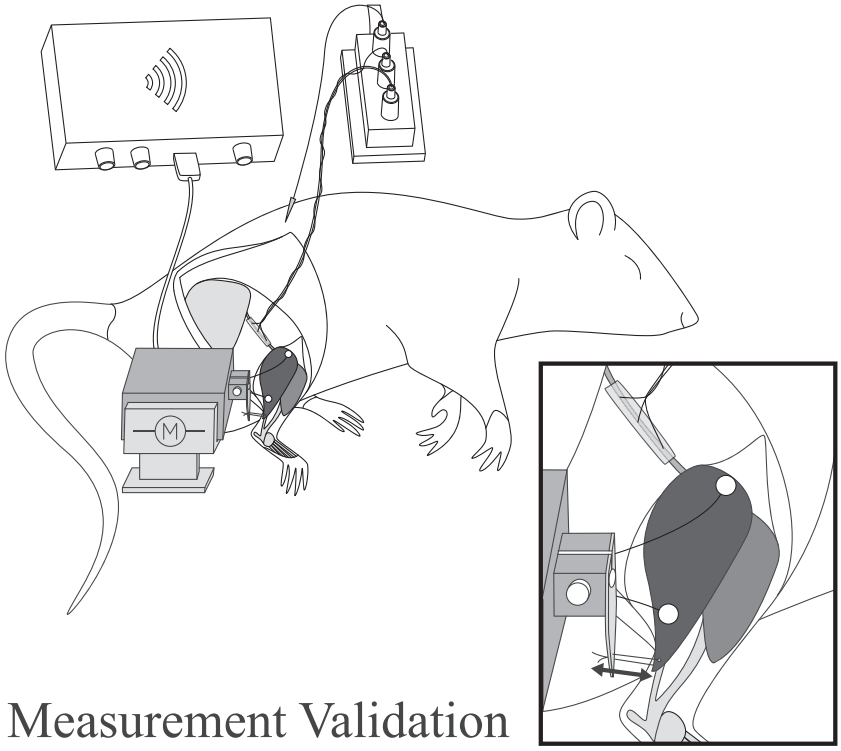

Figure 2. Experimental setup for measurement validation. A muscle tensioner was used to stretch the GSC through a series of ramp-and-holds, while muscle state was recorded via sonomicrometery (white circles in the muscle tissue), and ENG was recorded via a nerve cuff on the tibial nerve. (Artwork: Stephanie L Ku 2016).

of external stimulation or manipulation. The maximum and minimum distance signals from the LG sonomicrometery crystals during this cycling were analyzed to establish percent stretch metrics for the LG.

2.3. Validation of acquisition system

The following experiment was designed to ensure robustness in the ENG and sonomicrometery recording systems, as well as to establish a baseline for graded motor afferent response to LG muscle stretch. In 5 animals the gastrocnemius-soleus complex (GSC) was disinserted at the Achilles tendon, and isolated from the surrounding musculature. The knee joint was then pinned to the experimental surface, and the distal Achilles tendon was anchored to the lever arm of a dual-mode muscle tensioning system (305C-LR, Aurora Scientific) via 5-0 nylon suture (figure 2). Resting stretch in the instrumented GSC was adjusted by moving the lever arm until the force transducer in the muscle tensioning system showed a non-zero tension, indicating that there was no slack in the muscle. As a secondary form of validation, crystal readouts at this position were compared to resting values from the range-of-motion trial, and small adjustments were made to the lever arm until any discrepancy was eliminated.

A series of ramp-and-hold stretches were then carried out to each of 5 stretch magnitudes: 2, 4, 6, 8, and 9 mm, which was representative of the full range of muscle stretch achieved during passive joint cycling. In an attempt to standardize dynamic response characteristics, all dynamic trajectories (the 'ramps') were carried out at a constant velocity of 1 mm s^{-1}. This velocity was selected to be comparable to the slowest values presented in the literature [47], so as to preserve the characteristic dynamic response of the primary spindle afferents, but limit the impact of this response on the subsequent hold plateau. Stretch positions (the 'holds') were maintained for 5 s [31, 48]. A rest period of 10 s was allowed between subsequent ramp-and-hold trials. During the trials, force and length data were recorded from the muscle tensioner equipment. Sonomicrometery stretch data were simultaneously recorded from the crystals within the LG. Afferent electroneurography was recorded from the tibial nerve using a tripolar cuff electrode. Leads from the two outer electrode contacts were tied together and passed to one input of the differential amplifier; the lead from the middle electrode contact was passed to the other differential input [30]. Differential signals were pre-amplified (Grass P511 AC Amplifier, Grass Instruments), bandpass filtered (0.3–3 kHz), and amplified (RHD2000, Intan Technologies) before being recorded. 5 trials were performed for each stretch magnitude for each animal. System validation was based on (1) visual inspection of the ENG signal for a characteristic peak-plateau shape, (2) high fidelity of sonomicrometric measurements to ground-truth stretch measurement obtained via sensors within the muscle tensioner, and (3) a positive correlation between ENG amplitude and stretch magnitude.

2.4. Experimental paradigms

2.4.1. Native architecture. The following experiment was designed as a positive control, to which function of the AMI architecture was compared. In the remaining animals ($n = 5$),

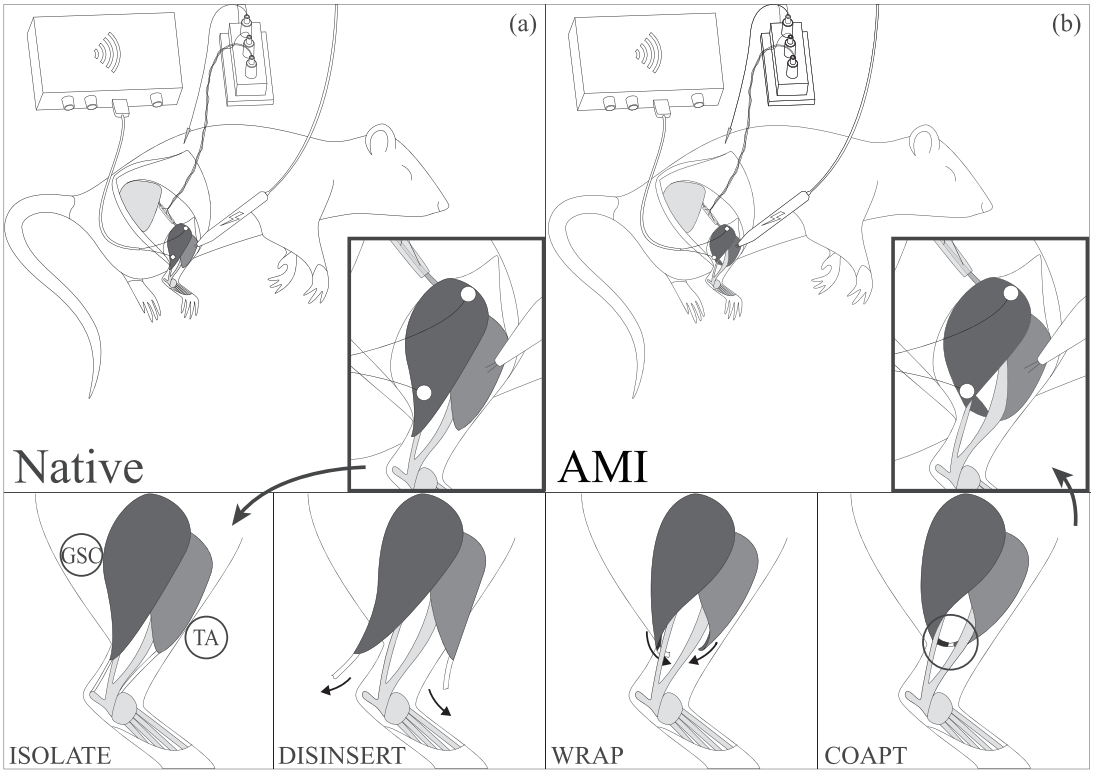

Figure 3. Experimental paradigms. With the musculature in (a) native and (b) AMI architectures, the TA was stimulated through a series of ramp-and-holds, while LG muscle state and ENG were recorded. White circles in the GSC represent sonomicrometery crystals. The bottom panel shows the surgical steps involved in building the AMI. (Artwork: Stephanie L Ku 2016).

with hindlimb musculature in its native architecture, a stimulating hook electrode was inserted into the TA muscle belly (figure 3(a)). Monophasic muscle stimulation was delivered by a commercial muscle stimulator (NL800, Digitimer), with stimulation parameters controlled digitally using a microcontroller. A heuristic control loop was enforced, with the LG sonomicrometery signal serving as feedback. LG muscle stretch (and consequently ankle position) was directly controlled by modulating TA stimulation parameters. Specifically, a proportional-integrative gain architecture modulated stimulation amplitude and pulse width within safe limits (amplitude from 0–3 mA, pulse width from 300–800 μs) to minimize the difference between the desired ramp-and-hold trajectories and actual LG stretch signals. Amplitude and pulse width were changed simultaneously and linearly, with abrupt output saturation at maximum values. Controller gains were tuned experimentally, for each animal, to optimize the balance between rise time and overshoot. All stimulation was delivered at 40 Hz, to ensure a fused tetanus.

With the hindlimb suspended above the table by a suture through the ankle joint capsule, the stimulation control system, acting on the TA, was used to perform a series of ramp-and-hold stretches of the GSC. A total of 90 ramp-and-hold stretches were carried out in the 5 animals, to various stretch magnitudes corresponding to approximately 20, 40, 60, 80, and 100 percent maximal stretch. All controls were enforced in units of percent crystal strain, defined as the difference between the instantaneous crystal distance and the rest crystal distance, divided by the rest crystal distance. Dynamic trajectories were carried out at a constant velocity of 1% crystal strain per second. Stretch positions were maintained for 5 s. A rest period of 10 s was allowed between subsequent ramp-and-hold trials. During the trials, sonomicrometery stretch data were recorded from the crystals within the LG. Afferent neural activity was recorded from the tibial nerve using the tripolar cuff electrode and amplifier configuration described above, with the addition of a sample-and-hold blanking circuit after pre-amplification. This blanking circuit was used to silence the preamplifier for a 1 ms window after each stimulation pulse. Although this 1 ms window was sufficient to prevent amplifier saturation, it did not entirely eliminate stimulus artifact; a 5 ms blanking window was enforced in software during processing to ensure complete elimination of the stimulus artifact.

2.4.2. AMI architecture. Once data collection in the native muscle geometry was complete, the AMI was constructed in the instrumented hindlimb of each animal (figure 3(b)). The distal Achilles and TA tendons were first identified and transected near their insertions. The GSC and TA were then isolated from surrounding tissues and wrapped medially in opposite directions around the tibia. The distal tendons were coapted medially with 5-0 nylon suture, with special attention given to ensuring that the resulting crystal signals at rest matched the rest signals from the physiological milieu. The full surgical paradigm is shown in figure 3.

The stimulation control system, acting on the TA, was again used to perform a series of ramp-and-hold stretches of

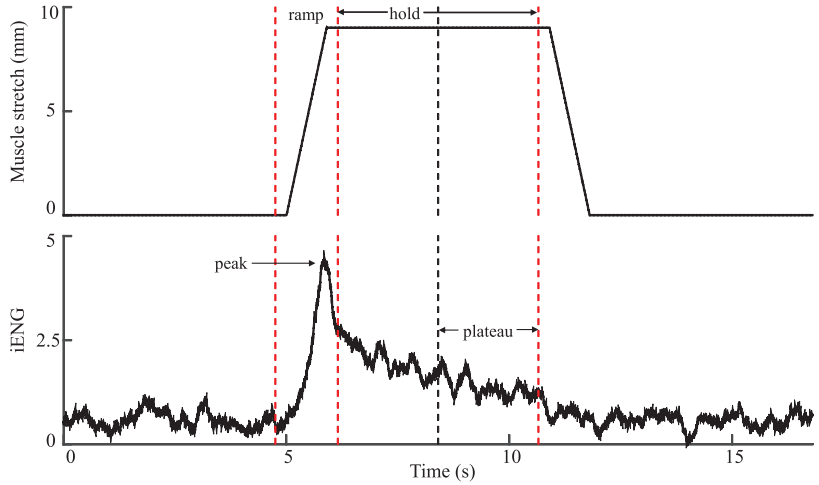

Figure 4. Typical iENG response during a single ramp-and-hold trial. Zero-velocity iENG amplitude is defined as the average iENG value during the second half of the hold. iENG signal is normalized to maximum zero-velocity plateau amplitude recorded for each animal.

the GSC. A total of 60 ramp-and-hold stretches were carried out in the 5 animals, to various stretch magnitudes. Target dynamic trajectories were carried out at a constant velocity of 1% crystal strain per second. It should be noted here that the range of motion for the AMI construct allowed for lower stretch magnitudes than the native architecture; this is explored in depth in the discussion section of this paper. Stretch positions were maintained for 5 s. A rest period of 10 s was allowed between subsequent ramp-and-hold trials. During the trials, sonomicrometery stretch data and afferent nerve signal were recorded as described in section 2.4.1. These data were then compared to those obtained from the native architecture; similarity amongst the two systems would imply that the AMI architecture is capable of replicating the physiological interaction between agonist and antagonist muscles.

To ensure blanking efficacy, after completion of the AMI experiment, the tibial nerve was transected distal to the nerve cuff. A ramp-and-hold series was then performed with parameters identical to those used for the AMI experiment, and both ENG and crystal strain were recorded.

2.5. Data storage and processing

Force and length data from the muscle tensioner system were stored at 10 kHz, and exported from proprietary software (DMC/DMA, Aurora Scientific). Sonomicrometery and ENG data were sampled on the Intan RHD2000 at 20 kHz. All data were processed in Matlab (Mathworks, Inc.). Sonomicrometery signals were smoothed with a 0.5 s sliding window, and baseline-drift corrected. To validate signal quality, ENG signal-to-noise ratio (SNR) was computed according to the analysis presented in [49]. Specifically, mean absolute value (MAV) was defined as the arithmetic mean of the rectified ENG signal. SNR was then computed as the ratio of the average MAV during passive motion of the joint to the average value of MAV during rest. This analysis produced an SNR of 3.57 dB, which is within the range of values seen for comparable trials in [49] (2.28 dB–3.82 dB). ENG signals were bandpass filtered (0.3–3 kHz, Butterworth), normalized, digitally rectified, and then bin integrated using a moving window of 250 ms to produce an integrated ENG (iENG) signal. Zero-velocity iENG amplitude was defined as $a_{\text{plateau}} - a_{\text{base}}$, where a_{base} is the average baseline amplitude of the iENG signal, and a_{plateau} is the mean amplitude during the second half of the 'hold' portion [31], as shown in figure 4.

3. Results

3.1. Validation of acquisition system

Figure 5 shows the results of a sample trial of the muscle tensioner experiment, which was used to validate the sonomicrometric measurement and ENG acquisition systems. ENG recordings were visually inspected for the peak-plateau shape characteristic of spindle afferent response to ramp-and-hold stretches.

To evaluate measurement accuracy, sonomicrometer distance signals were compared to lengths enforced on the muscle tensioner system. The smoothed sonomicrometer signal was normalized to maximum crystal strain, then scaled to fit the maximum stretch enforced on the muscle tensioner (9 mm). A trigger pulse from the muscle tensioner to the sonomicrometery recording system allowed for the two signals to be time-synced. A correlation analysis was then performed on the two signals from each trial. The correlation coefficients for each trial were averaged. The average coefficient of fit across all trials was $\overline{R} = 0.9897 \pm 0.0089$, providing strong evidence for crystal signal accuracy.

Figure 6 shows a regression analysis for normalized crystal strain values versus zero-velocity iENG amplitude. Samples were binned based on stretch magnitudes, and bin centers were regressed against zero-velocity plateau amplitude. Error bars on each point represent standard error within the bin. The coefficient of fit for the regression was .78.

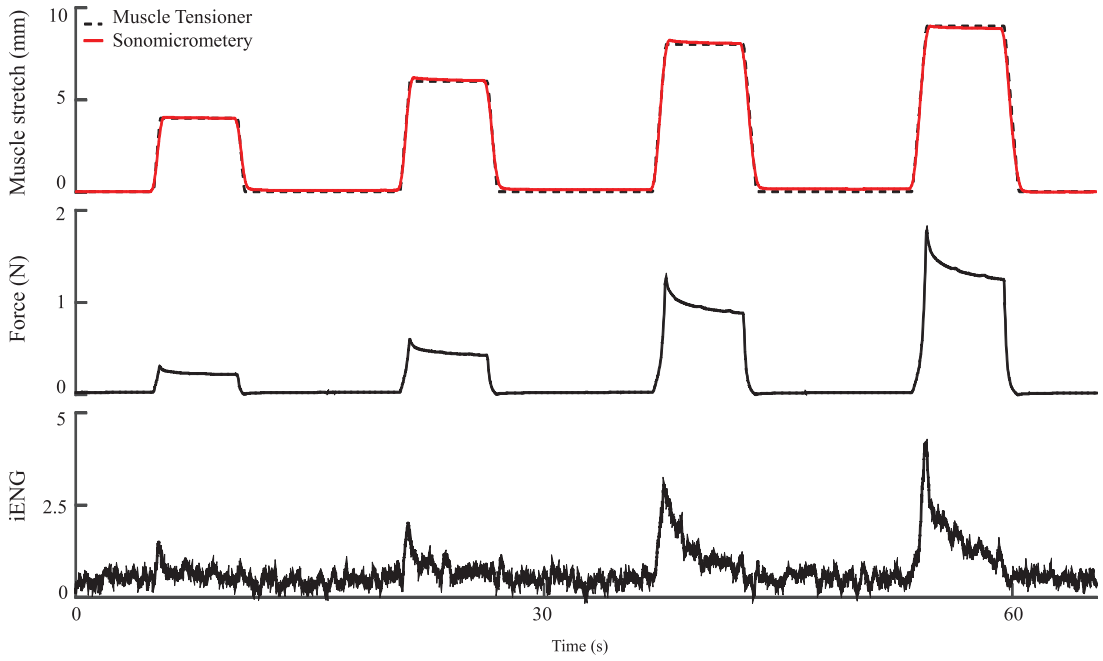

Figure 5. Results of the measurement validation experiments. iENG signal is normalized to maximum zero-velocity plateau amplitude recorded for each animal.

3.2. Closed-loop muscle state control

Sample position tracking trajectories for the closed-loop muscle state control system are shown in figure 7. PI gains were experimentally tuned for each animal to optimize the balance between rise time and overshoot. In the typical trial, performance in the AMI was characterized by slower reactivity, manifested in the plots as slower rise times and fall times. Steady state error was typically indicative of either physical limitations on muscle stretch, or muscle fatigue in the stimulated muscle, and was more prevalent in the AMI trials.

3.3. Afferent stretch response

Sample crystal and integrated ENG data for the native and AMI experiments are shown in figures 8(a) and (b). To account for changes in absolute crystal distances associated with the surgical change in muscular geometry, crystal strains were normalized to the maximum values achieved for the associated animal and muscle geometry paradigm (native or AMI). iENG values were normalized to the maximum zero-velocity iENG amplitude for each animal, because nerve cuffs did not change position between muscle geometry paradigms. Of particular note in these data is the preservation of characteristic peak-plateau responses to ramp-and-hold stretches in both the native and AMI paradigms. The post-nerve-transection iENG is shown in figure 8(c). The lack of neural signal present in these trials verified efficacy of the blanking system in eliminating stimulation artifact.

Regression analysis was performed in both experimental paradigms, comparing normalized crystal strain values against zero-velocity iENG amplitude (figure 8(d)). As above, samples were binned based on stretch values, and bin centers were regressed against discharge rates. Error bars on each point represent standard error within the bin. Coefficients of fit in the native and AMI architectures were similar to those seen in the muscle tensioner (R^2 of 0.95 and 0.80, respectively). The slope of the regression line for the AMI case (0.24) was lower than that for the native case (0.62), indicating that the native geometry was capable of provoking larger zero-velocity iENG amplitudes than the AMI geometry.

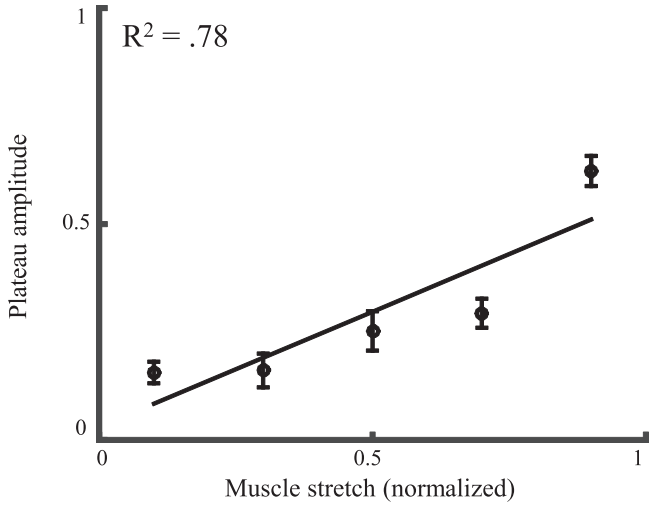

Figure 6. Regression of zero-velocity plateau amplitude versus normalized muscle stretch for the measurement validation experiments.

4. Discussion

4.1. Summary of results

In this paper, we present results demonstrating the potential of a novel surgical architecture to provide physiologically-relevant muscle-tendon proprioceptive feedback through

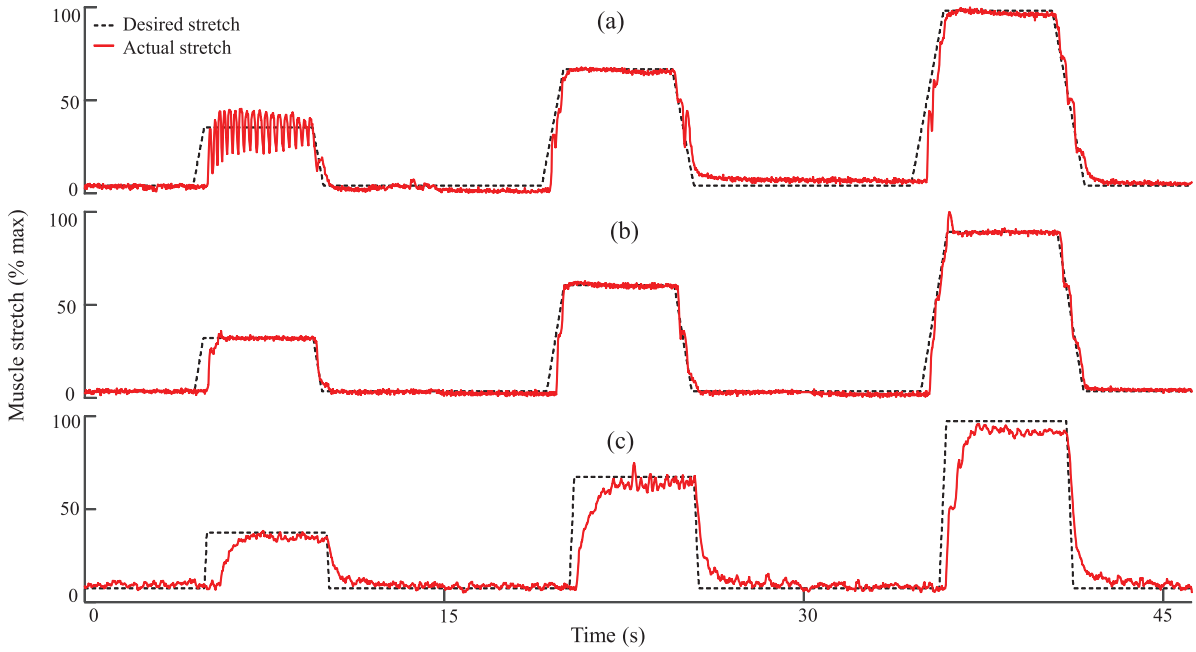

Figure 7. Tracking trajectories during closed-loop muscle stimulation control for the (a) native architecture typical case, (b) native architecture best case, and (c) AMI typical case. Muscle stretch is normalized as a percentage of the maximum stretch achieved for the associated muscle architecture.

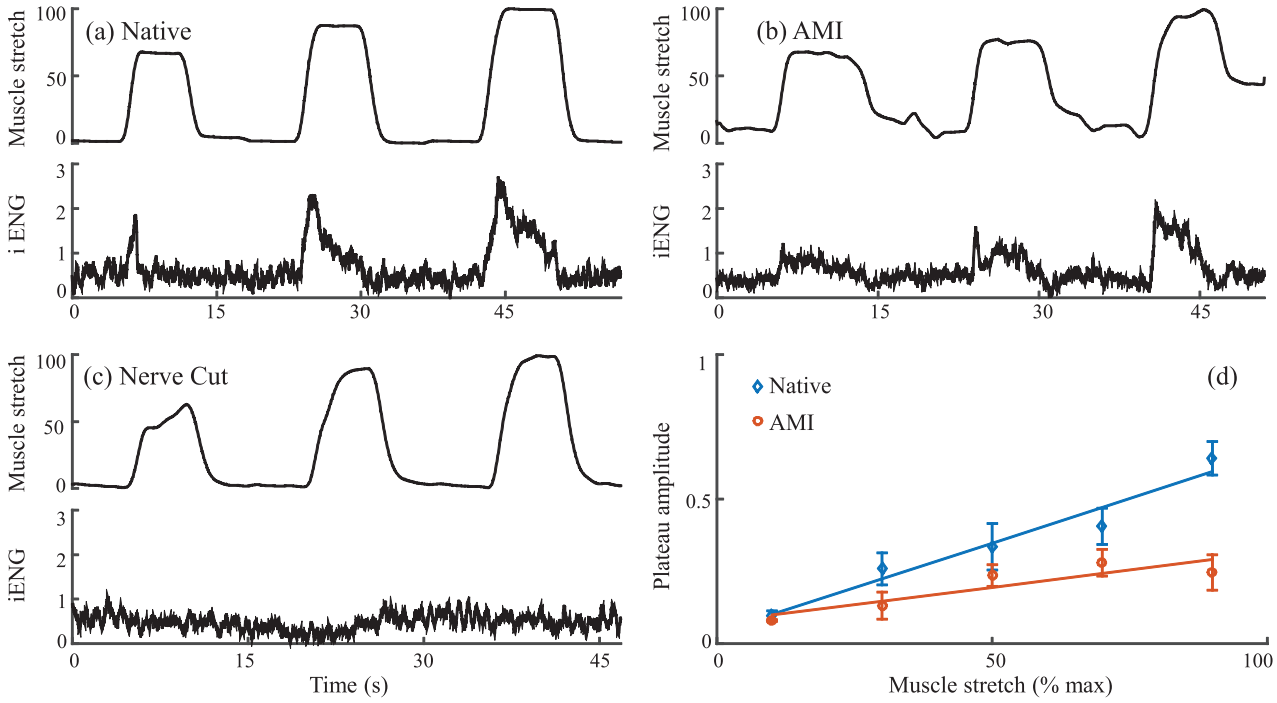

Figure 8. Experimental results comparing performance of the (a) native, (b) AMI, and (c) severed nerve architectures. Muscle stretch is normalized as a percentage of the maximum stretch achieved for the associated muscle architecture. iENG and plateau amplitudes are normalized to maximum zero-velocity plateau amplitude recorded for each animal. These data are combined across all animals in (d), which shows regression of zero-velocity plateau amplitude versus normalized muscle stretch for the native and AMI architectures.

native afferent channels. Specifically, two fundamental advancements were explored and validated. First, a closed-loop stimulation control system, based on reliable muscle stretch data from sonomicrometery crystals, was shown to provide robust control of an agonist–antagonist muscle pair. Second, the AMI demonstrated the capacity to provide sufficient agonist–antagonist coupling to evoke a graded spindle response in the antagonist's innervation nerve. This work represents the first step toward the long-term goal of a clinically-viable amputation paradigm for direct neural interfacing with advanced limb prostheses.

4.2. Translation of the AMI to human subjects

The AMI is designed for bi-directional neural communication with a bionic limb. The expected use case is as follows:

1. One AMI is surgically constructed for each degree-of-freedom of the prosthesis. Muscle electrodes and sonomicrometery crystals are placed within each muscle of each AMI. At rest, both the agonist and antagonist muscles of each AMI are at resting length and tension.
2. When joint motion is intended (either volitional or reflexive), the subject sends efferent neural commands to cause muscle contraction. EMG recorded from electrodes within the contracting muscle(s) and muscle fascicle length and contraction velocity are combined to generate a movement command to the prosthesis. There are several potential control architectures by which this movement command could be generated; herein, we have opted to present a method involving direct position-impedance modulation. In this approach, the angular position of each prosthetic joint is controlled by the arithmetic difference between the EMG intensity of the two muscles making up the AMI associated with that joint. Joint impedance is modulated by the common-mode signal of the two EMG intensities.
3. Natural contraction of the agonist muscle stretches the antagonist muscle and vice versa, as in the physiological milieu. Afferent signals from native mechanoreceptors within the natively-innervated agonist and antagonist muscles are interpreted by the subject as position and force sensation from the prosthesis.

This system also has the potential to provide force feedback from the prosthesis, through single-muscle FES. By stimulating the antagonist during natural agonist contraction, tension could be generated in the linked system to provide force feedback through the afferents of the agonist muscle and tendon. The incorporation of sonomicrometery and EMG from the agonist muscle into a neuromuscular model of force production (e.g. [50, 51]) as a feedback signal to the FES system would allow robust control of this afferent force sensation. It is important to note that such a system has implications for plausible efferent control architectures. Although the full exploration of these architectures falls outside the scope of the present work, one could imagine a system in which, for example, the controller described during step 2 above is used during free space control, where the FES system is inactive. The architecture could then shift to a single-muscle control paradigm, drawing EMG from the unstimulated, naturally-activated agonist muscle, when a force is applied to the limb (e.g. ground contact). Future research will evaluate how best to take advantage of the control opportunities provided by the AMI's unique preservation of functional agonist–antagonist muscle relationships.

This architecture provides several benefits over methodologies that rely on direct electrical stimulation of nervous tissue. The use of native mechanoreceptors to generate usable afferent signals from mechanical muscle strains obviates the need for complex, high-resolution neural stimulation. Contact between synthetic materials and nerve tissue is eliminated, instead relying on muscle-based electrodes for signal communication, which are more viable [12] and provide signals with an amplitude 100–1000× that of direct recording neural electrodes.

Although this work in an animal model represents only a first step in validating the efficacy of the AMI construct in providing graded muscle-tendon proprioceptive feedback, careful thought has been taken to address concerns of translatability. A primary concern is that the proposed surgical architecture would fundamentally interfere with socket-fitting practices by limiting the availability of soft tissues for distal bone coverage. It is our opinion that there exists sufficient redundancy in musculoskeletal physiology to allow deliberate selection of a subset of muscles that would make up the AMI for each degree of freedom, thereby preserving the remaining muscle tissue for purposes of traditional residuum-sculpting practices. This would allow rehabilitation to proceed according to standard socket-fitting protocols. Other concerns surrounding translation include excessive scarring, limb instability, and myoplastic integrity. Large animal trials are currently underway to explore the safety and integrity of this system in an amputation model; early indications are that none of these potential issues presents an insurmountable barrier.

4.3. Potential improvements and benefits inherent to translation

The relatively strong correlation of zero-velocity iENG amplitude to crystal strain in the AMI points to a functional relationship between stretch magnitude and afferent discharge, indicating the capacity of the AMI construct to provide graded stretch feedback. Although the correlation is slightly weaker in the AMI than for the native architecture, it mirrors the correlation observed using the muscle tensioner during validation trials. The lower slope, however, can likely be attributed to lower absolute stretch magnitudes, which may be the result of surgical manipulation of muscle attachment geometries during construction of the AMI.

One example of the ways in which muscle geometry impacts LG stretch magnitude becomes clear if we consider the physiological system in the context of simple machines; in this light, the foot serves as a lever of the first kind, with a pivot at the ankle joint. The ratio of effective ankle moment arms of the rat LG and TA during dorsiflexion, derived from data published in [52] and shown in figure 9(a), can be then interpreted as a simple transmission between the TA and LG muscle groups. The contraction magnitudes produced in the TA are amplified in LG stretch by the inverse of the transmission ratio. This amplification is no longer applied in the AMI architecture, because the ankle 'transmission' is bypassed when the muscles are surgically coapted. A relevant consideration is how these geometric constraints will affect system performance in the human physiology. In the human ankle, for instance, the transmission ratios from the muscles responsible for primary actuation (TA during dorsiflexion, and GSC during plantarflexion) to the associated antagonist muscles are shown in figures 9(b) and (c) (data from [53]). Physiological transmission ratios close to one indicate that bypassing the joint will have little effect on stretch profiles, while ratios greater than one indicate that the stretch within the AMI antagonist will be amplified when compared to stretch in the physiological milieu. In this latter case, the force-generating capacity of

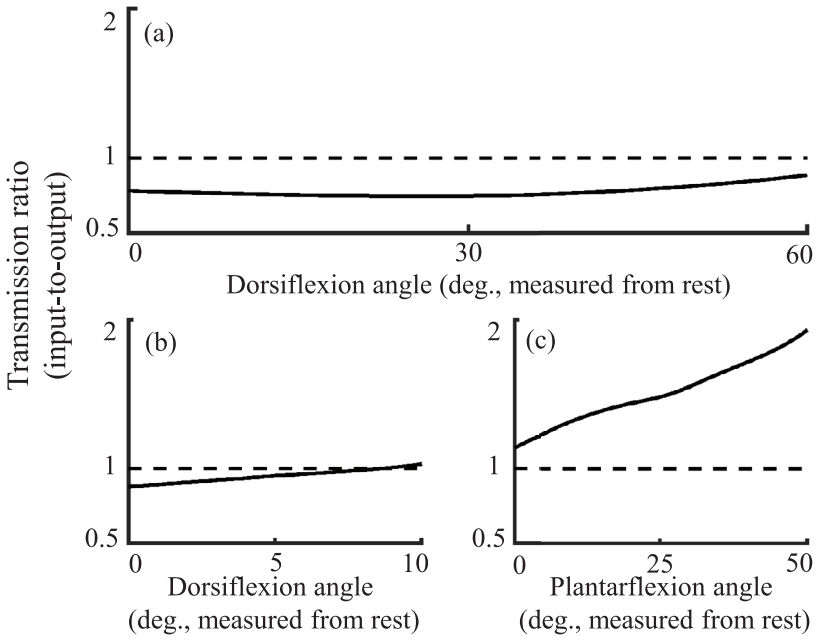

Figure 9. Effective transmission ratios linking agonist muscle contraction to antagonist muscle stretch in (a) rat dorsiflexion, (b) human dorsiflexion, and (c) human plantarflexion.

each muscle comes into consideration, as the stretch benefit is offset by a loss in mechanical advantage.

Friction also plays a role in limiting LG stretch. In the AMI, the wrapping of the LG and TA muscles around the bone creates a Capstan force opposing construct motion, which is absent in the native architecture. Simplifying the bone as a cylindrical wrapping surface, this force is proportional to $e^{\mu\theta}$, where μ is the coefficient of static friction and θ is the wrapping angle. As reported in [54], the frictional coefficient for muscle on bone is 0.29. With a wrapping angle of 180°, we calculate a Capstan gain of approximately 2.5, which would significantly impact sliding. One potential solution to this problem is to consider replacing the muscle-on-bone sliding surface with a physiologic sliding surface, which have significantly lower coefficients of friction. Tendons gliding on their synovial sheaths, for example, experience a frictional coefficient of 0.02–0.03 [55, 56], which would yield a Capstan gain of 1.06–1.1. This would significantly reduce the impact of friction on coupled agonist–antagonist motion in the AMI.

Adjustments to the stimulation paradigm may improve performance of the control system. Oscillation at low stretch magnitudes, as seen in figure 6(a), is likely the result of reverse-order fiber recruitment, which is a problem inherent to FES [57]. Because larger, stronger fibers are recruited first, high-resolution force control is difficult at low forces. It is our expectation that controller performance can be significantly improved with stimulation approaches that are not susceptible to the reverse-order recruitment problem, such as optical methods [58].

4.4. Expansion to regenerative approaches

Although the current work explores surgical constructs that are possible only in amputation cases in which native musculature remains functionally viable, the principles demonstrated herein have a much broader applicability. By integrating regenerative peripheral nerve interface technology [59], we envision the utilization of these methods in patients with pre-existing amputations. In this population, it will be possible to recreate viable agonist–antagonist muscle pairs at the distal ends of transected nerves, and link them together to reproduce the functionality that was validated in this study.

5. Conclusion

Lower extremity amputation is extremely prevalent, and current standards of clinical care leaves much to be desired. Lack of advancement in amputation surgery has contributed to a sub-optimal physiological setting in which researchers explore potential mechanisms for integration of bionic limbs with the peripheral nervous system. By addressing this issue at the point of clinical care, we have the potential to craft a residuum that is optimized for provision of graded proprioceptive afferent feedback through native neural pathways. Although the current work represents a simple proof-of-concept in an animal model, we anticipate that further development of the AMI will lead to necessary advancements in amputation surgery.

Acknowledgments

We thank Paul Cederna for his consultation on this project. We would also like to acknowledge Alex Harding for his preliminary work on stimulation modeling, Roman Stolyarov for his writing consultation, and Jennifer Haupt, Morgan Jamiel, and the MIT Division of Comparative Medicine for their contributions to animal work and care. Stephanie L Ku contributed original figures. This work was funded by the MIT Media Lab Consortium.

References

[1] Ziegler-Graham K, MacKenzie E, Ephraim P, Travison T and Brookmeyer R 2008 Estimating the prevalence of limb loss in the United States: 2005–2050 *Arch. Phys. Med. Rehabil.* **89** 422–9

[2] 2015 *Passport for the Orthopedic Boards and FRCS Examination* Ed C Mauffrey and D J Hak (Berlin: Springer)

[3] Rouse E J, Mooney L M and Herr H M 2014 Clutchable series-elastic actuator: Implications for prosthetic knee design *Int. J. Robot. Res.* **33** 1611–25

[4] Herr H M and Grabowski M 2012 Bionic ankle-foot prosthesis normalizes walking gait for persons with leg amputation *Proc. R. Soc.* B **279** 457–64

[5] Bellman R D, Holgate M A and Sugar T G 2008 SPARKy 3: design of an active robotic ankle prosthesis with two actuated degrees of freedom using regenerative kinetics *Proc. 2nd Biennial IEEE/RAS-EMBS Int. Conf. on Biomedical Robotics and Biomechatronics, BioRob 2008* pp 511–6

[6] Hargrove L J, Simon A M, Young A J, Lipschutz R D, Finucane S B, Smith D G and Kuiken T A 2013 Robotic leg control with EMG decoding in an amputee with nerve transfers *New Engl. J. Med.* **369** 1237–42

[7] Sup F, Bohara A and Goldfarb M 2008 Design and control of a powered transfemoral prosthesis *Int. J. Robot. Res.* **27** 263–73

[8] Huang S, Wensman J P and Ferris D P 2014 An experimental powered lower limb prosthesis using proportional myoelectric control *J. Med. Device.* **8** 024501

[9] Huang H and Kuiken T A 2009 A strategy for identifying locomotion modes using surface electromyography *IEEE Trans. Biomed. Eng.* **56** 65–73

[10] Brown B J, Iorio M L, Klement M, Conti Mica M R, El-Amraoui A, O'Halloran P and Attinger C E 2014 Outcomes after 294 transtibial amputations with the posterior myocutaneous flap *Int. J. Lower Extrem. Wounds* **13** 33–40

[11] Cao P and De Rango P 2010 Lower extremity amputation: techniques and results *Rutherford's Vasc. Surg.* **2** 1469–86

[12] Ortiz-Catalan M, Brånemark R, Håkansson B and Delbeke J 2012 On the viability of implantable electrodes for the natural control of artificial limbs: review and discussion *Biomed. Eng. Online* **11** 33

[13] Schultz A E and Kuiken T A 2011 Neural interfaces for control of upper limb prostheses: the state of the art and future possibilities *PMR* **3** 55–67

[14] Riemann B L and Lephart S M 2002 The sensorimotor system, part II: the role of proprioception in motor control and functional joint stability *J. Athl. Train.* **37** 80–4

[15] Kandel E R, Schwartz J H and Jessell T M 2013 The control of movement *Princ. Neural Sci.* **4** 1414

[16] Boyd I A and Roberts T D M 1953 Proprioceptive discharges from stretch-receptors in the knee-joint of the cat *J. Physiol.* **122** 38–58

[17] Skoglund S 1956 Anatomical and physiological studies of knee joint innervation in the cat *Acta Physiol. Scand.* **36** 1–100

[18] Burke D, Gandevia S C and Macefield G 1988 Responses to passive movement of receptors in joint, skin and muscle of the human hand *J. Physiol.* **402** 347–61

[19] Ochoa J and Torebjörk E 1983 Sensations evoked by intraneural microstimulation of single mechanoreceptor units innervating the human hand *J. Physiol.* **342** 633–54

[20] Macefield G, Gandevia S C and Burke D 1990 Perceptual responses to microstimulation of single afferents innervating joints, muscles and skin of the human hand *J. Physiol.* **429** 113–29

[21] Collins D F, Refshauge K M, Todd G and Gandevia S C 2005 Cutaneous receptors contribute to kinesthesia at the index finger, elbow, and knee *J. Neurophysiol.* **94** 1699–706

[22] Edin B B and Johansson N 19995 Skin strain patterns provide kinaesthetic information to the human central nervous system *J. Physiol.* **487** 243–51

[23] Proske U and Gandevia S C 2012 The proprioceptive senses: their roles in signaling body shape, body position and movement, and muscle force *Physiol. Rev.* **92** 1651–97

[24] Burgess P R and Clark F J 1969 Characteristics of knee joint receptors in the cat *J. Physiol.* **203** 317–35

[25] Burgess P, Wei J, Clark F and Simon J 1982 Signaling of kinesthetic information by peripheral sensory receptors *Annu. Rev. Neurosci.* **5** 171–87

[26] Hulliger M 1984 The mammalian muscle spindle and its central control *Rev. Physiol. Biochem. Pharmacol.* **101** 1–110

[27] Loeb G E 1984 The control and responses of mammalian muscle spindles during normally executed motor tasks *Exerc. Sport Sci. Rev.* **12** 157–204

[28] Boyd I and Gladden M 1985 *The Muscle Spindle* (London: Macmillan)

[29] Taylor A and Prochazka A 1981 *Muscle Receptors and Movement* (London: Macmillan)

[30] Riso R R, Mosallaie F K, Jensen W and Sinkjaer T 2000 Nerve cuff recordings of muscle afferent activity from tibial and peroneal nerves in rabbit during passive ankle motion *IEEE Trans. Rehabil. Eng.* **8** 244–58

[31] Edin B B and Vallbo A B 1990 Dynamic response of human muscle spindle afferents to stretch *J. Neurophysiol.* **63** 1297–306

[32] Jansen J K and Matthews P B 1962 The central control of the dynamic response of muscle spindle receptors *J. Physiol.* **161** 357–78

[33] Matthews P 1972 *Mammalian Muscle Receptors and Their Central Actions* (London: Arnold)

[34] Eklund G 1972 Position sense and state of contraction; the effects of vibration *J. Neurol. Neurosurg. Psychiatry* **35** 606–11

[35] Goodwin G M, Mccloskey D I and Matthews P B C 1972 The contribution of muscle afferents to kinaesthesia shown by vibration induced illusions of movement and by the effects of paralysing joint afferents *Brain* **95** 705–48

[36] Ribot-Ciscar E and Roll J P 1998 Ago-antagonist muscle spindle inputs contribute together to joint movement coding in man *Brain Res.* **791** 167–76

[37] Grigg P, Finerman G A and Riley L H 1973 Joint-position sense after total hip replacement *J. Bone Joint Surg. Am.* **55** 1016–25

[38] Wall P D and Noordenbos W 1977 Sensory functions which remain in man after complete transection of dorsal columns *Brain* **100** 641–53

[39] Ross E D, Kirkpatrick J B and Lastimosa A C B 1979 Position and vibration sensations: functions of the dorsal spinocerebellar tracts? *Ann. Neurol.* **5** 171–6

[40] Hogan N 1984 Adaptive control of mechanical impedance by coactivation of antagonist muscles *IEEE Trans. Automat. Control* **29** 681–90

[41] Dimitriou M 2014 Human muscle spindle sensitivity reflects the balance of activity between antagonistic muscles *J. Neurosci.* **34** 13644–55

[42] Goodwin G M, Mccloskey D I and Matthews P B C 1972 Proprioceptive illusions induced by muscle vibration: contribution by muscle spindles to perception? *Science* **175** 1382–4

[43] Tan D W, Schiefer M A, Keith M W, Anderson J R, Tyler J and Tyler D J 2014 A neural interface provides long-term stable natural touch perception *Sci. Transl. Med.* **6** 257ra138

[44] Griffiths R I 1997 Ultrasound transit time gives direct measurement of muscle fibre length *in vivo J. Neurosci. Methods* **21** 159–65
[45] Roberts T J 1997 Muscular force in running turkeys: the economy of minimizing work *Science* **275** 1113–5
[46] McGuigan M P, Yoo E, Lee D V and Biewener A A 2009 Dynamics of goat distal hind limb muscle-tendon function in response to locomotor grade *J. Exp. Biol.* **212** 2092–104
[47] Rosant C, Nagel M D and Pérot C 2007 Aging affects passive stiffness and spindle function of the rat soleus muscle *Exp. Gerontol.* **42** 301–8
[48] De-Doncker L, Picquet F, Petit J and Falempin M 2003 Characterization of spindle afferents in rat soleus muscle using ramp-and-hold and sinusoidal stretches *J. Neurophysiol.* **89** 442–9
[49] Raspopovic S, Carpaneto J, Udina E, Navarro X and Micera S 2010 On the identification of sensory information from mixed nerves by using single-channel cuff electrodes *J. Neuroeng. Rehabil.* **7** 17
[50] Hill A V 1938 The heat of shortening and the dynamic constants of muscle *Proc. R. Soc.* B **126** 136–95
[51] Lee S S M, Arnold A S, Miara M D B, Biewener A A and Wakeling J M 2013 Accuracy of gastrocnemius muscles forces in walking and running goats predicted by one-element and two-element Hill-type models *J. Biomech.* **46** 2288–95
[52] Johnson W L, Jindrich D L, Roy R R and Edgerton V R 2008 A three-dimensional model of the rat hindlimb: musculoskeletal geometry and muscle moment arms *J. Biomech.* **41** 610–9
[53] Rugg S G, Gregor R J, Mandelbaum B R and Chiu L 1990 *In vivo* moment arm calculations at the ankle using magnetic resonance imaging (MRI) *J. Biomech.* **23** 495–501
[54] Castel D 2010 Measurements of the static friction coefficient between bone and muscle tissues *J. Biomech. Eng.* **132** 084502
[55] Amadio P C 2013 Gliding resistance and modifications of gliding surface of tendon: clinical perspectives *Hand Clin.* **29** 159–66
[56] Amadio P C 2005 Friction of the gliding surface: implications for tendon surgery and rehabilitation *J. Hand Ther.* **18** 112–9
[57] Hamada T, Kimura T and Moritani T 2004 Selective fatigue of fast motor units after electrically elicited muscle contractions *J. Electromyogr. Kinesiol.* **14** 531–8
[58] Llewellyn M E, Thompson K R, Deisseroth K and Delp S L 2010 Orderly recruitment of motor units under optical control *in vivo Nat. Med.* **16** 1161–5
[59] Kung T A, Langhals N B, Martin D C, Johnson P J, Cederna P S and Urbanchek M G 2014 Regenerative peripheral nerve interface viability and signal transduction with an implanted electrode *Plast. Reconstr. Surg.* **133** 1380–94